NANO LETTERS

pubs.acs.org/NanoLett Letter

Point-of-Care Pathogen Testing Using Photonic Crystals and Machine Vision for Diagnosis of Urinary Tract Infections

Haoran Liu,[§] Zhihao Li,[§] Ruichen Shen, Zhiheng Li, Yanbing Yang,* and Quan Yuan*

Cite This: *Nano Lett.* 2021, 21, 2854−2860 Read Online

ACCESS | Metrics & More | Article Recommendations | Supporting Information

ABSTRACT: Urinary tract infections (UTIs) caused by bacterial invasion can lead to life-threatening complications, posing a significant health threat to more than 150 million people worldwide. As a result, there is need for accurate and rapid diagnosis of UTIs to enable more effective treatment. Described here is an intelligent diagnostic system constructed for bacterial detection using an immunobiosensor, signal-amplification biochip, and image processing algorithm based on machine vision. This prototype can quickly detect bacteria by collection of enhanced luminescence enabled by the photonic crystals integrated into the biochip. By use of a machine vision algorithm, the very small luminescence signals are analyzed to provide a low detection limit and wide dynamic range. This sensor system can offer an affordable, accessible, and user-friendly digital diagnostic solution, possibly suitable for wearable technology, that could improve treatment of this challenging disease.

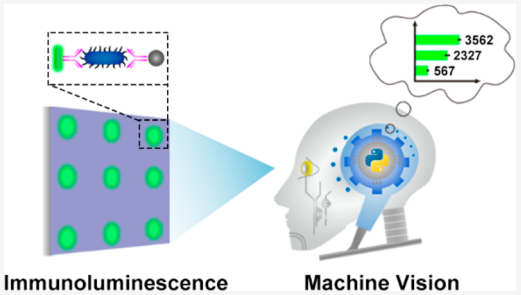

KEYWORDS: *urinary tract infection, bacterial detection, immunoluminescence, biochip, machine vision*

Urinary tract infections (UTIs), the inflammations caused by pathogenic bacterial invasion in urinary tracts, have been considered to be one of the most common disease-related infections worldwide.[1,2] As a significant threat to human health, UTIs can cause pyelonephritis, urosepsis, premature birth, and even death.[3−8] Thus, periodic checkups are essential for UTI patients after recovery due to the high recurrence rates.[9,10] However, urine culture, as the diagnostic gold standard for UTIs, requires time-consuming processes, leading to considerable economic burden to patients.[11−13] Development of an immediate, convenient, and economical urinalysis method will be of extreme significance for the rapid diagnosis and early intervention of UTIs.

In recent years, immunoluminescence has been widely used in the fields of biosensing and clinical diagnosis due to its high sensitivity and specificity.[14−22] Moreover, the visual signal produced by luminescence can be observed by the naked eye, making it suitable to establish point-of-care (POC) testing.[23−27] However, reliance on manual observation rather than spectrophotometric measurement leads to large subjective uncertainty, as well as difficulty in reporting quantitative data.

As one type of digital technology, machine vision (MV) has emerged as "computer eyes" to simulate human visual function and objective perception.[28,29] The MV algorithm can report accurate and reliable results after rapid processing and analysis of digital images captured by cameras.[30−32] Furthermore, the results can be easily quantified due to the robust computing algorithms, thus eliminating subjective errors in manual observations.[33,34] In this regard, MV is capable of more reliable POC applications and thus is promising for developing "family doctor" diagnosis.[35−37]

In this paper, we integrate a Python image algorithm into photonic crystal-based biochips to construct an MV-based diagnostic system for detecting bacteria in urine samples. As shown in Scheme 1, antibody-modified Zn_2GeO_4:Mn nano-

Scheme 1. Illustration of MV-Based Diagnostic System Achieving Immunoluminescence Analysis for Detecting Bacteria in Urine

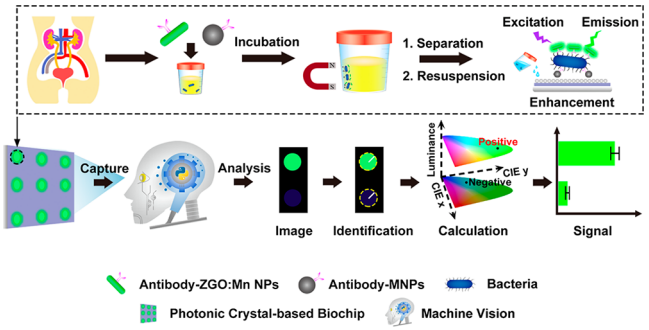

Received: December 16, 2020
Revised: March 21, 2021
Published: March 26, 2021

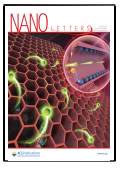

https://doi.org/10.1021/acs.nanolett.0c04942
Nano Lett. 2021, 21, 2854−2860

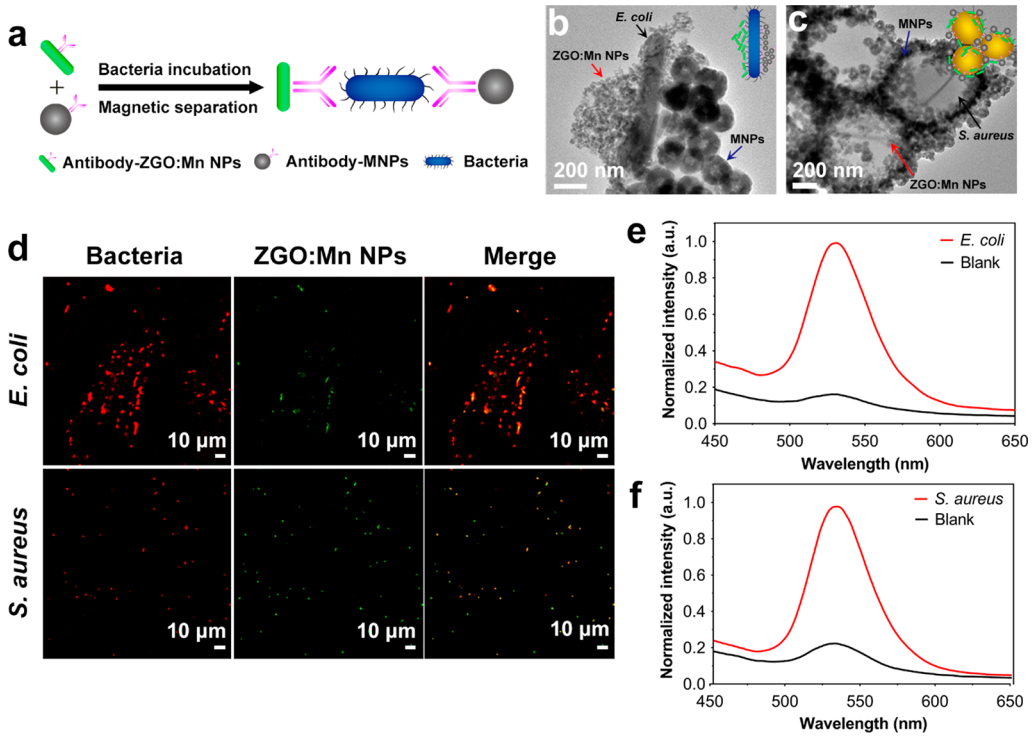

Figure 1. (a) Schematic illustration of bacterial detection by sandwich-based immunoluminescence assay. TEM images of (b) *E. coli* and (c) *S. aureus* captured and recognized by antibody-modified ZGO:Mn NPs and MNPs. (d) Confocal microscopy images of *E. coli* and *S. aureus* labeled by antibody-modified ZGO:Mn NPs: red, bacteria; green, ZGO:Mn NPs. Luminescence spectra of (e) ZGO:Mn NPs-*E. coli*-MNPs and (f) ZGO:Mn NPs-*S. aureus*-MNPs immunocomplexes.

particles (ZGO:Mn NPs) specifically bind and capture target bacteria by antibody−antigen recognition. After magnetic separation and resuspension, ZGO:Mn NPs emit enhanced luminescence enabled by photonic crystals on the biochips. After capture, the luminescence is easily identified from raw images and is converted into digital signals by machine vision algorithms. This cooperation between algorithm and biosensor results in a low detection limit and wide dynamic range in quantitative urinalysis. For patients with chronic diseases, such as hypertension and diabetes, this MV-based diagnostic system is expected to provide a high-quality, reliable, and affordable tool for modern health management and personalized medicine in the big data era.

RESULTS AND DISCUSSION

A sandwich-based immunoluminescence assay was used for detection of bacteria in urine. To perform this assay, both magnetic nanoparticles (MNPs, carboxyl-modified Fe_3O_4 nanoparticles) and luminescent ZGO:Mn NPs were prepared and then functionalized with antibodies against the pathogenic bacteria. As shown in Figure S1, transmission electron microscopy (TEM) images indicate that MNPs are well-dispersed with a uniform size of about 100 nm. In addition, ZGO:Mn NPs, prepared using a previously reported hydrothermal method,[38,39] show a well-dispersed nanorod shape with an average length of about 50 nm (Figures S2 and S3). The X-ray powder diffraction (XRD) pattern in Figure S4 also indicates that the peaks of as-prepared NPs match well with those of standard ZGO:Mn crystals [JCPDS No. 11-0687]. The luminescence properties of ZGO:Mn NPs were also investigated. As shown in Figure S5, the luminescence spectrum of ZGO:Mn NPs shows a strong emission band that is located at 535 nm, and the inset picture shows strong green luminescence under UV excitation. These results confirmed that the luminescent ZGO:Mn NPs were successfully synthesized.

Next, ZGO:Mn NPs were modified with carboxyl groups and further functionalized with antibodies to bacteria. The changes in ζ potentials demonstrate the successful modifications of carboxyl groups on the surfaces of ZGO:Mn NPs and MNPs (Figure S6). Also, bicinchoninic acid (BCA) protein assay was used to confirm the presence of antibodies on the NP surfaces. The antibodies of bacteria lead to significant changes of absorbance at 562 nm (Figure S7). All these results suggest that the ZGO:Mn NPs and MNPs were successfully prepared and that antibodies of bacteria were functionalized onto the nanoparticles.

Then, the feasibility of bacteria detection was investigated using sandwich-based immunoluminescence assay. The principle of detection is illustrated in Figure 1a. In the presence of bacteria, antibody-modified ZGO:Mn NPs and MNPs bind to the surfaces of bacteria to form immunocomplexes through antibody−antigen recognition. TEM and confocal microscopy were utilized to characterize the formation of immunocomplexes. As shown in Figure 1b and Figure S8, several ZGO:Mn NPs and MNPs are tightly attached with *E. coli*, confirming the interaction of nanomaterials and *E. coli*. Similar immunocomplexes were also observed for *S. aureus* (Figure 1c). Additionally, confocal images (Figure 1d) show that the luminescence of ZGO:Mn NPs overlaps the fluorescence of propidium iodide (PI)-stained bacteria, indicating that bacteria can be specifically labeled by antibody-modified ZGO:Mn NPs. These results suggest that immunocomplexes were formed successfully.

https://doi.org/10.1021/acs.nanolett.0c04942
Nano Lett. 2021, 21, 2854−2860

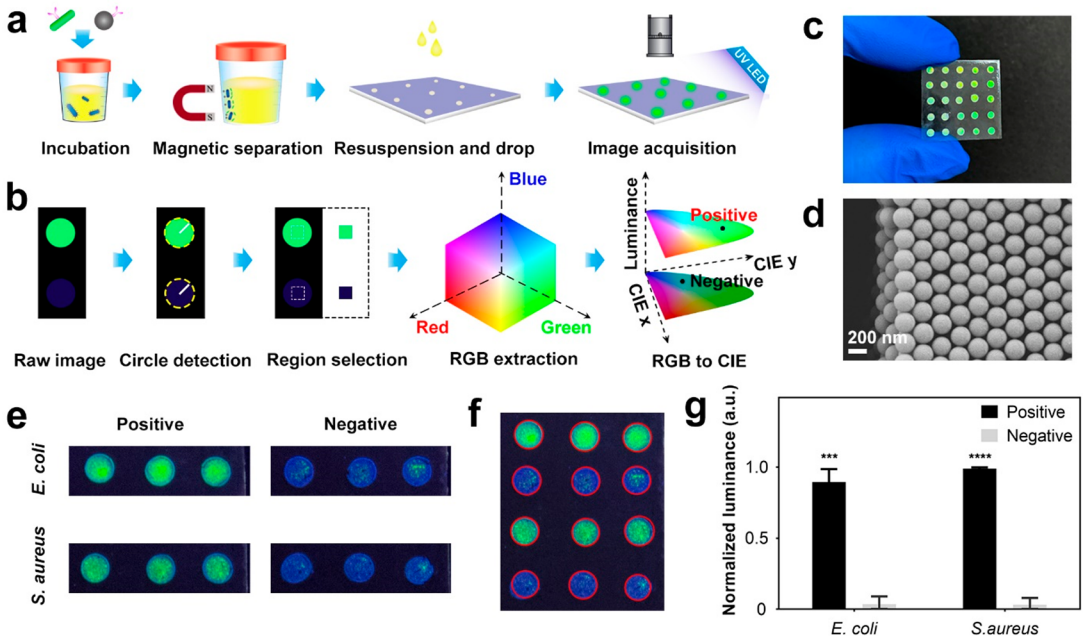

Figure 2. (a) Illustration of immunoluminescence assay supported by PC-based biochips. (b) Workflow of immunoluminescence image analysis by Python algorithm. (c) Photograph of PC-based biochip. (d) SEM image of PC dots. (e) Raw images of PC dots, where positive samples and negative samples were dropped on the biochip when detecting *E. coli* and *S. aureus*. (f) Recognition results of PC dots by image algorithm. (g) Normalized luminance values of positive samples and negative samples for the detection of *E. coli* and *S. aureus*. The luminance values of negative samples were normalized against the highest positive samples. Data are mean values ± sd (n = 3, three technical replicates). Statistical significance was calculated by Student's t test (unpaired, two-tailed): $^{**}P < 0.01$, $^{***}P < 0.001$, $^{****}P < 0.0001$.

Furthermore, luminescence emission was utilized to confirm the detection of bacteria. In the presence of *E. coli*, a strong emission band peaking at 535 nm is observed, while no obvious emission band is found for negative samples (Figure 1e). Similarly, the strong emission peak can be observed in *S. aureus* samples, while only a weak peak is present in the blank spectrum (Figure 1f).

After confirmation of the luminescence emission of the ZGO:Mn NPs-bacteria-MNPs immunocomplexes, detection parameters including reaction time, the usage of ZGO:Mn NPs, and MNPs were optimized (Figure S9). The detection limit was evaluated by measuring different concentrations of samples containing 10^5−10^8 CFU/mL of bacteria as presented in Figure S10 and Figure S11. Additionally, the specificity of this strategy was tested by choosing two interfering bacteria, *Sal. typhimurium* (G-) and *Sar. lutea* (G+) as controls. The luminescence intensities from *Sal. typhimurium* and *Sar. lutea*-containing samples approximated that of the blank, much lower than those of *E. coli*- and *S. aureus*-containing samples (Figure S12). The above-mentioned results clearly indicate that the immunosandwich strategy based on ZGO:Mn NPs can be used for bacterial detection.

To design a POC urinalysis, the sandwich immunoluminescence strategy was combined with a signal-amplifying biochip to construct a portable device (Figure 2a). Photonic crystals (PCs) are spatially highly ordered nanomaterials with periodic structures.[40−42] Due to photonic band-gap properties, PCs can reflect light with specific wavelengths and thus enhance the intensity of light.[43−45] Inspired by these unique optical properties, PC-based biochips were fabricated as optical signal amplifiers (Figure S13). As shown in Figure 2c, PC dots are arranged in an array on a portable biochip that can be held between the thumb and forefingers. Scanning electron microscopy (SEM) images show that PC dots exhibit highly ordered layered structures built by stacking of close-packed arrangement of polystyrene (PS) nanospheres (Figure 2d and Figure S14). The transmission band of the PC dot overlaps the luminescence emission band of ZGO:Mn NPs (Figure S15), thus confirming that PC dots can reflect the luminescence of ZGO:Mn NPs. To ensure that this light manipulation can amplify detection signals, droplets containing immunocomplexes were dripped onto the surface of PC dots of biochip. The luminescence intensity of immunocomplexes on the biochip was increased more than 4-fold (Figure S16). These results show that PC-based biochips can be utilized as efficient signal amplifiers to enhance luminescence.

To realize real-time and digital detection, a Python algorithm was developed to process luminescence enabled by the PC-based biochip (Figure 2b), and a digital single-lens reflex camera was used to collect luminescence images. As shown in Figure S17, Hough circle transformation in the Python algorithm could detect the edge, find the center, and measure the radius of the circle. As a result, this algorithm could automatically recognize circular luminescence dots in luminescence images. After that, square test regions, using the circular radius as the side length, were selected at the center of the circular luminescence dot (Figure 2b and Figure S17). The average RGB values were extracted from test regions and transformed into average chromaticity values (x, y) and luminance values (Y). As a result, each circular luminescence dot was converted into each data point in the Commission Internationale de L'Eclairage (CIE xyY) color space (Figure S18). In CIE xyY color space, the intensity of light is equivalent to luminance and wavelength determines chromaticity values.[46,47] Since intensity is independent of wavelength, luminance (Y) is orthogonal to and would not be affected by chromaticity values (x, y) (Figure 2b).[48] For our immunosandwich strategy, the emission wavelength of immunocom-

https://doi.org/10.1021/acs.nanolett.0c04942
Nano Lett. 2021, 21, 2854−2860

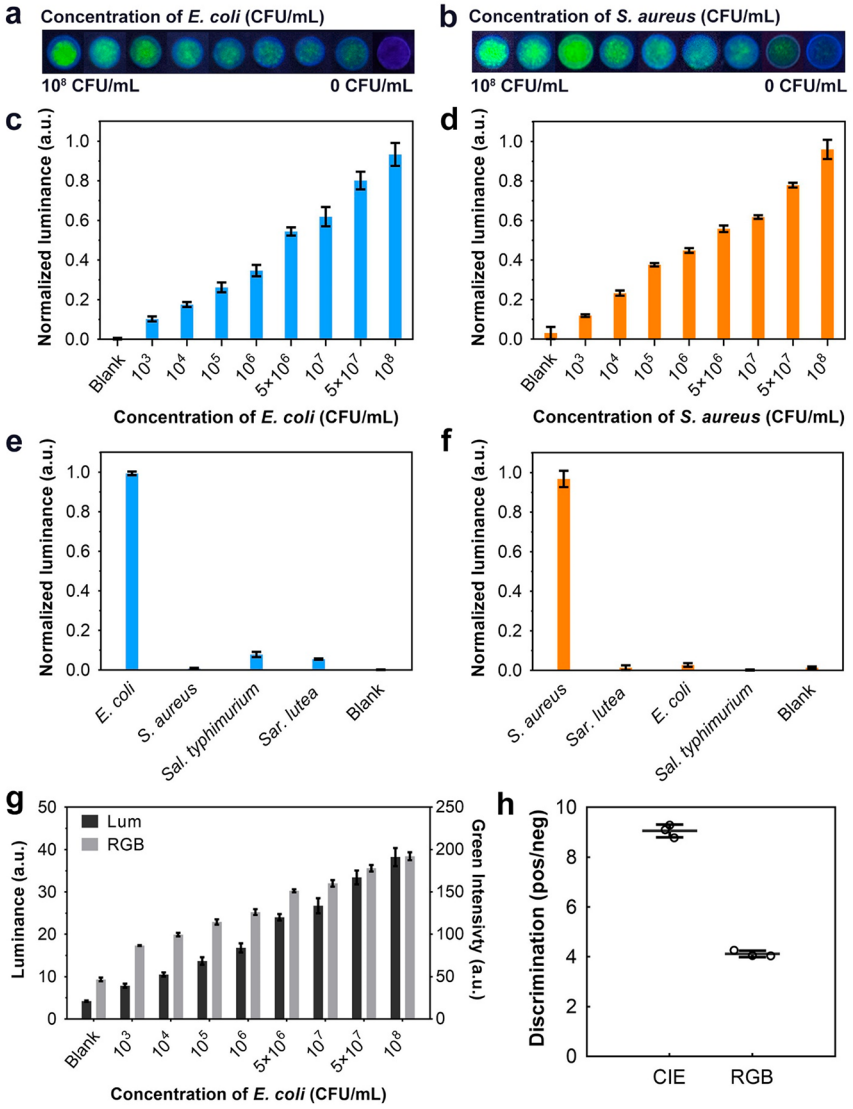

Figure 3. Visualized pictures for detection of (a) *E. coli* or (b) *S. aureus* at different concentrations by the MV-based detection system. Normalized luminance values output by the MV-based detection system in the presence of (c) *E. coli* or (d) *S. aureus* at different concentrations (from 10^3 to 10^8 CFU/mL). The signal responses to interfering bacteria of MV-based detection system when detecting (e) *E. coli* or (f) *S. aureus*. The concentrations of *E. coli* or *S. aureus* and interfering bacteria are all 10^7 CFU/mL. (g) Comparison of luminance values and green channel intensities as output signals of MV-based detection system. (h) Discrimination values of image analysis in CIE-*xyY* color space and RGB color space. The luminance values of samples with various bacterial concentrations were normalized against the value for the highest bacterial concentration. Data are mean values ± sd (n = 3, three technical replicates).

plexes is fixed, and only the emission intensity changes with different concentrations of bacteria (Figures S10 and S11). Therefore, chromaticity values (x, y) are almost unchanged and luminance (Y) is the only variable. On the basis of this, the luminance (Y) value was adopted to calculate the luminescence signal intensity in our algorithm. After positive samples and negative samples were dropped on the PC-based biochip, the performance of the image algorithm was investigated by processing collected luminescence images. All luminescence dots and nonluminescence dots in Figure 2e were easily recognized by the Python algorithm (Figure 2f). After calculation, the chromaticity values and luminance were obtained (Figure 2g and Table S1). As shown in Table S1, negative samples with no obvious emission, and positive samples with green light emission exhibited different chromaticity values. More importantly, positive samples exhibited much higher luminance values than negative samples (Figure 2g). All these results demonstrate that this Python algorithm, combined with PC-based biochips, can be used for bacterial detection.

After construction of the MV-based detection system by integrating the Python algorithm into a PC-based biochip, the detection sensitivity, dynamic range, and specificity of this detection system were investigated. First, a series of urine samples containing different concentrations of *E. coli* or *S. aureus* were tested. As shown in Figure 3a and Figure 3b, the visualized picture shows that PC dots detected different bacterial concentrations by emitting visible green luminescence with different intensities. After luminescence images were obtained and processed and quantitative relationships were obtained as shown in Figure 3c and 3d, the analysis results showed that the detection limit of *E. coli* is 10^3 CFU/mL (Figure 3c). It is worth mentioning that the brightness differences between samples with 10^3–10^5 CFU/mL of *E. coli*

https://doi.org/10.1021/acs.nanolett.0c04942
Nano Lett. 2021, 21, 2854−2860

are difficult to observe by naked eye but could be distinguished by the machine vision algorithm. This indicates that the MV-based detection system exhibits higher resolution than manual observation for low-concentration samples. Similarly, Figure 3d shows that the detection limit of *S. aureus* is as low as 10^3 CFU/mL. As shown in Table S2, our obtained detection limits are comparable to those of some previously reported methods and thus are suitable for the requirements of bacterial detection.

The specificity of the method was also investigated. Figure 3e shows that only *E. coli* can be detected by the MV-based detection system when the corresponding antibody is used. Also, the specificity tests indicate that only *S. aureus* can be detected with high luminance values (Figure 3f) when the *anti-S. aureus* antibody is used. Additionally, the output detection signal was compared with the green channel intensity to show the sensitivity of our detection system (Figure 3g). With increasing concentration of *E. coli*, luminance values rise more rapidly than green channel intensities. To evaluate this difference, the ratios of signal intensities from the sample with the highest concentration of *E. coli* and the blank sample were calculated as discrimination values in the two methods of image analysis. As shown in Figure 3h, the discrimination value of our system is more than twice that of RGB analysis. This significant improvement in the dynamic range of detection signals favors the distinction between positive and negative samples. All these results demonstrate that the MV-based detection system exhibits high sensitivity and excellent specificity for bacterial detection.

To further investigate the potential application of the MV-based detection system in UTI diagnosis, 15 urine samples were collected from adults of different genders and then tested by the system. Epidemiological research has shown that the incidence rates of UTIs in adult women are higher than the incidence rates in men.[49] Considering this, more female volunteers were chosen to donate urine samples (volunteer information in Table S3). As previously reported, the colony count of Gram-negative bacteria of $>10^5$ CFU/mL was acknowledged as the standard for UTI-positive.[50−53] Thus, urine samples were spiked with *E. coli* suspensions to ensure that the total concentrations were 10^5 CFU/mL after mixing, and these samples were considered as positive samples. At the same time, urine samples without *E. coli* were considered negative samples. All positive samples and negative samples were subsequently tested in parallel by urine culture and the MV-based detection system. The diagnosis results are shown in Figure 4a. The urine samples 2, 3, 5−9, 12, 13, and 15 tested positive according to the MV-based detection system. Meanwhile, the urine culture also reported that almost all these samples had bacterial concentrations of $>10^5$ CFU/mL. The exception was sample 3 with bacterial concentration of $<10^5$ CFU/mL, possibly due to accidental decrease of bacterial activity in the urine culture. Except for sample 3, UTI diagnoses by the MV-based detection system were consistent with those from urine culture. Additionally, the MV-based detection system provides significant differences between positive and negative samples (Figure 4b), and these results are comparable to those reported by urine culture (Figure 4c). Moreover, the distinction between positive and negative samples is independent of volunteer gender (Figure 4d), showing that the MV-based detection system works regardless of gender. Receiver operating characteristic (ROC) analysis showed that the MV-based detection system has the same

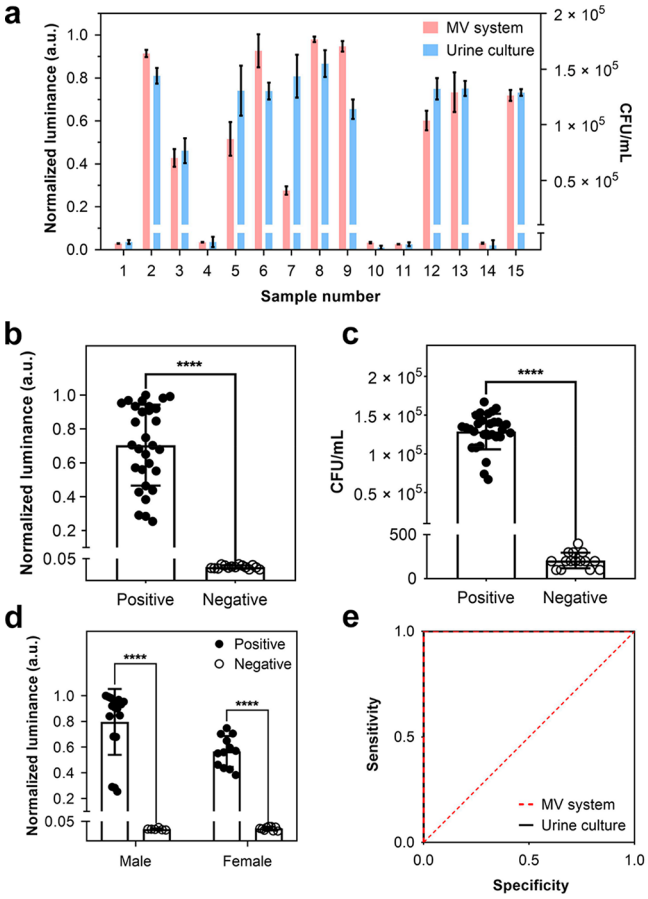

Figure 4. (a) Diagnostic report for urine samples tested by urine culture and MV-based detection system. (b) Normalized luminance values of positive samples and negative samples tested by MV-based detection system. (c) Colony forming units per milliliter (CFU/mL) reported by urine culture after positive samples and negative samples were cultured for 48 h. (d) Normalized luminance values of samples collected from volunteers with different genders. (e) Receiver operating characteristic (ROC) curves of UTI diagnoses acquired from urine culture and MV-based detection system. The luminance values of negative samples were normalized against the highest positive sample values. Data are mean values ± sd (n = 3, three technical replicates). Statistical significance was calculated by Student's t test (unpaired, two-tailed): $^{**}P < 0.01$, $^{***}P < 0.001$, $^{****}P < 0.0001$.

sensitivity and specificity as the urine culture method (Figure 4e). More importantly, the analysis time was shortened by the MV-based detection system (Figure S19). Overall, the MV-based detection system can be considered as a rapid, intelligent, and accurate POC diagnosis method for UTIs.

CONCLUSION

A machine vision-based diagnostic system was developed for digital detection of bacteria in human urine. As luminescence materials to label bacteria, ZGO:Mn NPs specifically bind to bacteria by antibody−antigen recognition. PC-based biochips capable of optical enhancement output amplified detection signals for the Python image algorithm. As the core of the machine vision system, image resolution of the algorithm is superior to that of manual observation. This diagnostic system, combining an immunobiosensor, optical enhancement, and image algorithm, provides very satisfying detection performance. Consequently, this system offers a portable, intelligent,

https://doi.org/10.1021/acs.nanolett.0c04942
Nano Lett. 2021, 21, 2854−2860

and user-friendly diagnostic tool that meets the health needs to operate anytime and anywhere. Additionally, for other luminescence nanoparticles that can bind with targeted molecules, such as antibodies and aptamers, this machine vision system has excellent prospect for quantification of luminescence signals in biological analysis and medical diagnosis. With the rapid development of deep learning, this software−hardware cooperative system not only inspires potential design ideas for self-diagnosis of chronic diseases but also is highly promising for improving the accuracy and efficiency of medical diagnosis in specialized medicine.

■ ASSOCIATED CONTENT

Supporting Information

The Supporting Information is available free of charge at https://pubs.acs.org/doi/10.1021/acs.nanolett.0c04942.

Experimental materials and methods; TEM images of MNPs; TEM images, XRD pattern, and photoluminescence spectrum of ZGO:Mn NPs; ζ potentials and bicinchoninic acid protein assays for ZGO:Mn NPs and MNPs with different modifications; TEM images of immunocomplexes; optimization of detection parameters; luminescence spectra, linear relationships, and specificity tests obtained for bacterial detection; illustrations of the fabrication of PC-based biochip, recognition process of PC dots and color space conversion; SEM images of PC dots; enhanced ability and transmittance spectrum of the PC-based biochip; illustration of analysis time using urine culture and MV system; chromaticity values (x, y) calculated by Python program; comparison of our method to previously reported pathogen detection methods; information about volunteers donating urine samples (PDF)

■ AUTHOR INFORMATION

Corresponding Authors

Yanbing Yang − *Key Laboratory of Biomedical Polymers of Ministry of Education, College of Chemistry and Molecular Sciences, School of Microelectronics, Wuhan University, Wuhan 430072, China*; Email: yangyanbing@whu.edu.cn

Quan Yuan − *Key Laboratory of Biomedical Polymers of Ministry of Education, College of Chemistry and Molecular Sciences, School of Microelectronics, Wuhan University, Wuhan 430072, China; Institute of Chemical Biology and Nanomedicine, State Key Laboratory of Chemo/Biosensing and Chemometrics, College of Chemistry and Chemical Engineering, Hunan University, Changsha 410082, China*; orcid.org/0000-0002-3085-431X; Email: yuanquan@whu.edu.cn

Authors

Haoran Liu − *Key Laboratory of Biomedical Polymers of Ministry of Education, College of Chemistry and Molecular Sciences, School of Microelectronics, Wuhan University, Wuhan 430072, China*

Zhihao Li − *Key Laboratory of Biomedical Polymers of Ministry of Education, College of Chemistry and Molecular Sciences, School of Microelectronics, Wuhan University, Wuhan 430072, China*

Ruichen Shen − *Institute of Chemical Biology and Nanomedicine, State Key Laboratory of Chemo/Biosensing and Chemometrics, College of Chemistry and Chemical Engineering, Hunan University, Changsha 410082, China*

Zhiheng Li − *Key Laboratory of Biomedical Polymers of Ministry of Education, College of Chemistry and Molecular Sciences, School of Microelectronics, Wuhan University, Wuhan 430072, China*

Complete contact information is available at: https://pubs.acs.org/10.1021/acs.nanolett.0c04942

Author Contributions

[§]Haoran Liu and Zhihao Li contributed equally to this work.

Notes

The authors declare no competing financial interest.

■ ACKNOWLEDGMENTS

This work was supported by the National Key Research and Development Program of China (Grant 2017YFA0208000) and the Natural Science Foundation of China (Grants 21904100 and 21904033). Q.Y. thanks the large-scale instrument and equipment sharing foundation of Wuhan University.

■ REFERENCES

(1) Schollum, D. J. B.; Walker, P. R. J. Adult Urinary Tract Infection. *Br. J. Hosp. Med.* **2012**, *73*, 218−223.

(2) Klein, R. D.; Hultgren, S. J. Urinary Tract Infections: Microbial Pathogenesis, Host-pathogen Interactions and New Treatment Strategies. *Nat. Rev. Microbiol.* **2020**, *18*, 211−226.

(3) Al-Hasan, M. N.; Eckel-Passow, J. E.; Baddour, L. M. Bacteremia Complicating Gram-negative Urinary Tract Infections: A Population-based Study. *J. Infect.* **2010**, *60*, 278−285.

(4) Foxman, B.; Brown, P. Epidemiology of Urinary Tract Infections. *Infect. Dis. Clin. N. Am.* **2003**, *17*, 227−241.

(5) Bonkat, G.; Cai, T.; Veeratterapillay, R.; Bruyere, F.; Bartoletti, R.; Pilatz, A.; Koves, B.; Geerlings, S. E.; Pradere, B.; Pickard, R.; Wagenlehner, F. M. E. Management of Urosepsis in 2018. *Eur. Urol. Focus.* **2019**, *5*, 5−9.

(6) Wagenlehner, F. M.; Pilatz, A.; Naber, K. G.; Weidner, W. Therapeutic Challenges of Urosepsis. *Eur. J. Clin. Invest.* **2008**, *38*, 45−49.

(7) Katchman, E. A.; Milo, G.; Paul, M.; Christiaens, T.; Baerheim, A.; Leibovici, L. Three-day vs Longer Duration of Antibiotic Treatment for Cystitis in Women: Systematic Review and Meta-analysis. *Am. J. Med.* **2005**, *118*, 1196−1207.

(8) Jolley, J. A.; Kim, S.; Wing, D. A. Acute Pyelonephritis and Associated Complications During Pregnancy in 2006 in US Hospitals. *J. Matern.-Fetal Neonat. Med.* **2012**, *25*, 2494−2498.

(9) Foxman, B. Urinary Tract Infection Syndromes: Occurrence, Recurrence, Bacteriology, Risk factors, and Disease Burden. *Infect. Dis. Clin. N. Am.* **2014**, *28*, 1−13.

(10) Epp, A.; Larochelle, A.; Lovatsis, D.; Walter, J.-E.; Easton, W.; Epp, A.; Farrell, S. A.; Girouard, L.; Gupta, C.; Harvey, M.-A.; Larochelle, A.; Robert, M.; Ross, S.; Schachter, J.; Schulz, J. A.; Wilkie, D.; Ehman, W.; Domb, S.; Gagnon, A.; Hughes, O.; Konkin, J.; Lynch, J.; Marshall, C. Recurrent Urinary Tract Infection. *J. Obstet. Gynaecol. Can.* **2010**, *32*, 1082−1090.

(11) Foxman, B.; Barlow, R.; D'Arcy, H.; Gillespie, B.; Sobel, J. D. Urinary Tract Infection: Self-Reported Incidence and Associated Costs. *Ann. Epidemiol.* **2000**, *10*, 509−515.

(12) Freedman, A. L.; Urologic Diseases in America Project. Urologic Diseases in North America Project: Trends in Resource Utilization for Urinary Tract Infections in Children. *J. Urol.* **2005**, *173*, 949−954.

(13) Schmiemann, G.; Kniehl, E.; Gebhardt, K.; Matejczyk, M. M.; Hummers-Pradier, E. The Diagnosis of Urinary Tract Infection: A Systematic Review. *Dtsch. Arztebl. Int.* **2010**, *107*, 361−367.

(14) Zirath, H.; Schnetz, G.; Glatz, A.; Spittler, A.; Redl, H.; Peham, J. R. Bedside Immune Monitoring: An Automated Immunoassay Platform for Quantification of Blood Biomarkers in Patient Serum within 20 minutes. *Anal. Chem.* **2017**, *89*, 4817−4823.
(15) Sayyadi, N.; Justiniano, I.; Connally, R. E.; Zhang, R.; Shi, B.; Kautto, L.; Everest-Dass, A. V.; Yuan, J.; Walsh, B. J.; Jin, D.; Willows, R. D.; Piper, J. A.; Packer, N. H. Sensitive Time-Gated Immunoluminescence Detection of Prostate Cancer Cells Using a TEGylated Europium Ligand. *Anal. Chem.* **2016**, *88*, 9564−9571.
(16) Su, X.-L.; Li, Y. Quantum Dot Biolabeling Coupled with Immunomagnetic Separation for Detection of *Escherichia coli* O157:H7. *Anal. Chem.* **2004**, *76*, 4806−4810.
(17) Zhou, X.; Luo, B.; Kang, K.; Ma, S.; Sun, X.; Lan, F.; Yi, Q.; Wu, Y. Multifunctional Luminescent Immuno-magnetic Nanoparticles: Toward Fast, Efficient, Cell-friendly Capture and Recovery of Circulating Tumor Cells. *J. Mater. Chem. B* **2019**, *7*, 393−400.
(18) Mondal, M.; Liao, R.; Xiao, L.; Eno, T.; Guo, J. Highly Multiplexed Single-Cell In Situ Protein Analysis with Cleavable Fluorescent Antibodies. *Angew. Chem., Int. Ed.* **2017**, *56*, 2636−2639.
(19) Gao, L.; Yang, Q.; Wu, P.; Li, F. Recent Advances in Nanomaterial-enhanced Enzyme-linked Immunosorbent Assays. *Analyst* **2020**, *145*, 4069−4078.
(20) Scott, D.; Dikici, E.; Ensor, M.; Daunert, S. Bioluminescence and Its Impact on Bioanalysis. *Annu. Rev. Anal. Chem.* **2011**, *4*, 297−319.
(21) Wu, L.; Li, G.; Xu, X.; Zhu, L.; Huang, R.; Chen, X. Application of Nano-ELISA in Food Analysis: Recent Advances and Challenges. *TrAC, Trends Anal. Chem.* **2019**, *113*, 140−156.
(22) Cheng, Y.; Xie, H.; Sule, P.; Hassounah, H.; Graviss, E. A.; Kong, Y.; Cirillo, J. D.; Rao, J. Fluorogenic Probes with Substitutions at the 2 and 7 Positions of Cephalosporin are Highly BlaC-specific for Rapid Mycobacterium Tuberculosis Detection. *Angew. Chem., Int. Ed.* **2014**, *53*, 9360−9364.
(23) Upaassana, V. T.; Ghosh, S.; Chakraborty, A.; Birch, M. E.; Joseph, P.; Han, J.; Ku, B. K.; Ahn, C. H. Highly Sensitive Lab on a Chip (LOC) Immunoassay for Early Diagnosis of Respiratory Disease Caused by Respirable Crystalline Silica (RCS). *Anal. Chem.* **2019**, *91*, 6652−6660.
(24) Roda, A.; Michelini, E.; Cevenini, L.; Calabria, D.; Calabretta, M. M.; Simoni, P. Integrating Biochemiluminescence Detection on Smartphones: Mobile Chemistry Platform for Point-of-need Analysis. *Anal. Chem.* **2014**, *86*, 7299−7304.
(25) Tabatabaee, R. S.; Golmohammadi, H.; Ahmadi, S. H. Easy Diagnosis of Jaundice: A Smartphone-Based Nanosensor Bioplatform Using Photoluminescent Bacterial Nanopaper for Point-of-Care Diagnosis of Hyperbilirubinemia. *ACS Sens.* **2019**, *4*, 1063−1071.
(26) Tian, Y.; Zhang, L.; Wang, H.; Ji, W.; Zhang, Z.; Zhang, Y.; Yang, Z.; Cao, Z.; Zhang, S.; Chang, J. Intelligent Detection Platform for Simultaneous Detection of Multiple MiRNAs Based on Smartphone. *ACS Sens.* **2019**, *4*, 1873−1880.
(27) Tenda, K.; van Gerven, B.; Arts, R.; Hiruta, Y.; Merkx, M.; Citterio, D. Paper-Based Antibody Detection Devices Using Bioluminescent BRET-Switching Sensor Proteins. *Angew. Chem., Int. Ed.* **2018**, *57*, 15369−15373.
(28) Wu, Y.; Lu, Y. An Intelligent Machine Vision System for Detecting Surface Defects on Packing Boxes Based on Support Vector Machine. *Meas. Control* **2019**, *52*, 1102−1110.
(29) Davies, E. R. The Application of Machine Vision to Food and Agriculture: A Review. *Imaging Sci. J.* **2009**, *57*, 197−217.
(30) Sun, X.; Chen, K.; Berg, E.; Magolski, J. Predicting Fresh Beef Color Grade Using Machine Vision Imaging and Support Vector Machine (SVM) Analysis. *J. Anim. Vet. Adv.* **2011**, *10*, 1504−1511.
(31) Abdullah, M. Z.; Aziz, S. A.; Dos Mohamed, A. M. Quality Inspection Of Bakery Products Using A Color-based Machine Vision System. *J. Food Qual.* **2000**, *23*, 39−50.
(32) Zhou, J.; Lin, P. T. Midinfrared Multispectral Detection for Real-Time and Noninvasive Analysis of the Structure and Composition of Materials. *ACS Sens.* **2018**, *3*, 1322−1328.
(33) Vithu, P.; Moses, J. A. Machine Vision System for Food Grain Quality Evaluation: A Review. *Trends Food Sci. Technol.* **2016**, *56*, 13−20.
(34) Patel, A. K.; Chatterjee, S.; Gorai, A. K. Development of Machine Vision-based Ore Classification Model Using Support Vector Machine (SVM) Algorithm. *Arabian J. Geosci.* **2017**, *10*, 107.
(35) Veli, M.; Ozcan, A. Computational Sensing of *Staphylococcus aureus* on Contact Lenses Using 3D Imaging of Curved Surfaces and Machine Learning. *ACS Nano* **2018**, *12*, 2554−2559.
(36) Tek, F. B.; Dempster, A. G.; Kale, I. Computer Vision for Microscopy Diagnosis of Malaria. *Malar. J.* **2009**, *8*, 153.
(37) Steenhoek, L. W.; Misra, M. K.; Hurburgh, C. R., Jr.; Bern, C. J. Implementing A Computer Vision System For Corn Kernel Damage Evaluation. *Appl. Eng. Agric.* **2001**, *17*, 235.
(38) Wang, J.; Ma, Q.; Liu, H.; Wang, Y.; Shen, H.; Hu, X.; Ma, C.; Yuan, Q.; Tan, W. Time-Gated Imaging of Latent Fingerprints and Specific Visualization of Protein Secretions via Molecular Recognition. *Anal. Chem.* **2017**, *89*, 12764−12770.
(39) Wang, J.; Ma, Q.; Zheng, W.; Liu, H.; Yin, C.; Wang, F.; Chen, X.; Yuan, Q.; Tan, W. One-Dimensional Luminous Nanorods Featuring Tunable Persistent Luminescence for Autofluorescence-Free Biosensing. *ACS Nano* **2017**, *11*, 8185−8191.
(40) Fenzl, C.; Hirsch, T.; Wolfbeis, O. S. Photonic Crystals for Chemical Sensing and Biosensing. *Angew. Chem., Int. Ed.* **2014**, *53*, 3318−3335.
(41) Shang, L.; Fu, F.; Cheng, Y.; Wang, H.; Liu, Y.; Zhao, Y.; Gu, Z. Photonic Crystal Microbubbles as Suspension Barcodes. *J. Am. Chem. Soc.* **2015**, *137*, 15533−15539.
(42) Zhang, Z.; Chen, Z.; Sun, L.; Zhang, X.; Zhao, Y. Bio-inspired Angle-independent Structural Color Films with Anisotropic Colloidal Crystal Array Domains. *Nano Res.* **2019**, *12*, 1579−1584.
(43) Hou, J.; Zhang, H.; Yang, Q.; Li, M.; Song, Y.; Jiang, L. Bio-inspired Photonic-crystal Microchip for Fluorescent Ultratrace Detection. *Angew. Chem., Int. Ed.* **2014**, *53*, 5791−5795.
(44) Ye, B.; Ding, H.; Cheng, Y.; Gu, H.; Zhao, Y.; Xie, Z.; Gu, Z. Photonic Crystal Microcapsules for Label-free Multiplex Detection. *Adv. Mater.* **2014**, *26*, 3270−3274.
(45) Yin, Z.; Zhu, Y.; Xu, W.; Wang, J.; Xu, S.; Dong, B.; Xu, L.; Zhang, S.; Song, H. Remarkable Enhancement of Upconversion Fluorescence and Confocal Imaging of PMMA Opal/$NaYF_4$:Yb^{3+}, Tm^{3+}/Er^{3+} Nanocrystals. *Chem. Commun.* **2013**, *49*, 3781−3783.
(46) Jha, S. N. *Nondestructive Evaluation of Food Quality: Theory and Practice*; Springer-Verlag: Berlin, Germany, 2010; pp17−72.
(47) Hunt, R. W. G.; Pointer, M. R. *Measuring Colour*; John Wiley & Sons: New York, 2011; pp19−72.
(48) Priye, A.; Bird, S. W.; Light, Y. K.; Ball, C. S.; Negrete, O. A.; Meagher, R. J. A Smartphone-Based Diagnostic Platform for Rapid Detection of Zika, Chikungunya, and Dengue Viruses. *Sci. Rep.* **2017**, *7*, 44778.
(49) Flores-Mireles, A. L.; Walker, J. N.; Caparon, M.; Hultgren, S. J. Urinary Tract Infections: Epidemiology, Mechanisms of Infection and Treatment Options. *Nat. Rev. Microbiol.* **2015**, *13*, 269−284.
(50) Burd, E. M.; Kehl, K. S. A Critical Appraisal of the Role of the Clinical Microbiology Laboratory in the Diagnosis of Urinary Tract Infections. *J. Clin. Microbiol.* **2011**, *49*, S34−S38.
(51) Cornaglia, G.; Courcol, R.; Hermann, J. L. *European Manual of Clinical Microbiology*; European Society of Clinical Microbiology and Infectious Diseases: Basel, Switzerland, 2012; pp133−143.
(52) Pezzlo, M. Laboratory Diagnosis of Urinary Tract Infections: Guidelines, Challenges, and Innovations. *Clin. Microbiol. Newsletter* **2014**, *36*, 87−93.
(53) Oyaert, M.; Van Meensel, B.; Cartuyvels, R.; Frans, J.; Laffut, W.; Vandecandelaere, P.; De Beenhouwer, H.; BILULU Study Group.. Laboratory Diagnosis of Urinary Tract Infections: Towards a BILULU Consensus Guideline. *J. Microbiol. Methods* **2018**, *146*, 92−99.

https://doi.org/10.1021/acs.nanolett.0c04942
Nano Lett. 2021, 21, 2854−2860